## ORIGINAL ARTICLE

# The effect of alkaline earth metals (Magnesium and Calcium) on Hydrogen storage efficiency of alanate nanopowders

*Navid Hosseinabadi\**

*Department of Material Engineering and Metallurgy, Faculty of Engineering, IAU-Shiraz Branch, Shiraz, Iran*

**Abstract**

Different Aluminum: alkaline earth metal atomic weight ratios effects on structure transformations in alanates nanopowders were studied. Changes in crystal structures from alane to alanates by increasing alkaline earth metals dopants in the mixture with slight changes in crystal structures from rhombohedral centered – trigonal (alane) to trigonal (magnesium alanate), and monoclinic (calcium alanate), while thermal behavior alters from one step dissociation at ~150 ºC with ~8.1 wt% hydrogen release in alane to the two steps hydrogen releases in magnesium alanate at 130 and 285 ºC with 7 and 2.1 wt% changes, and to the three steps hydrogen releases in calcium alanate at 127, 260, and 328 ºC with 1.7, 2.1, and 4 wt% changes were indicated. Residual phases after dissociation are formed in aluminum and magnesium alloying systems and intermetallic phases like $Mg_2Al_3$ and $Mg_{17}Al_{12}$ with no sign of oxide formation and pure aluminum, $Al_4Ca$, $Al_2Ca$ intermetallic phases and Ca in aluminum: Calcium system.

**How to cite this article**
*Hosseinabadi N, Sarraf MamoorY R. The effect of alkaline earth metals (Magnesium and Calcium) on hydrogen storage efficiency of alanate nanopowders. Int. J. Nano Dimens., 2018; 9 (1): 41-57.*

## INTRODUCTION

Most Aluminum based hydrides are known as acceptable hydrogen carriers with high hydrogen gravimetric contents due to their high hydrogen density and low hydrogen desorption temperatures and have drawn much attention as solid-state hydrogen storage [1,2]. For example, Alane ($AlH_3$) has found potential applications as solid hydrogen storage, chemical catalysts, explosives, propellants and pyrotechnics, and as a powerful reducing agent with seven crystal polymorphs (α - α′ - β - γ - ζ - δ - ε) and variety of crystal structures from trigonal, hexagonal, to orthorhombic. The most stable phase structure is α and the other phases decompose to this structure with no $H_2$ loss during these transformations [3-5].

Alane was mostly synthesized by wet chemical process, producing alane-ether complex within a solvent by reaction between aluminum chloride and $(C_2H_5)_2O$. Same synthesis can be carried out by its elements under high hydrogen pressures near 2.5 GPa [4]. The Products are very temperature and humidity sensitive, which makes it difficult to introduce additional alkaline and alkaline earth elements, also known as aluminum alanates [6]. A mechano-chemical synthesis process (MCSP) for alane has been introduced which involves the mechanical initiation of the reaction between aluminum chloride and $NaAlH_4$ [7-8]. In MCSP, ball milling promotes the reaction in a mixture of reactive powders. Enhanced reaction rates can be achieved during high energy milling as a result of micro-structural refinement and mixing processes accompanying with repeated fracture, cold welding, and deformation of particles during collision events. These events can cause the initiation of a solidstate displacement reaction during the milling process [5, 8-10] which can result in nano-sized particles down to 4nm. Products can be separated from precursors or [7] being embedded within large rby-products phases or attached to precursors. Mechanical millingis used for mechano-chemical synthesis of nanoparticles because it can mix the reactants

\* Corresponding Author Email: *hosseinabadi@iaushiraz.ac.ir*

and form nano sized mixtures which enhances the chemical reactivity leading to a chemical reaction between the reactants and products formation. Process can be controlled by milling factors like: the volume fraction of the by-product formation, milling time, milling collision energy (ball-to-powder weight ratio and ball size distribution [11]) and milling atmosphere [12].

Magnesium and calcium alanates, based on alane hydrides, are the most interesting compounds with high hydrogen contents and moderate dehydrogenation temperatures. These materials showed multiple step decomposition temperatures and enthalpies. The preparation of complex aluminum hydrides from a stoichiometric mixture of alkaline alanates and metal salts via MCSP, results in complex structures based on $AlH_4$ tetrahedrons as shown in the equation below [8]:

$Li/NaAlH_4 + MeCl_2 / MeCl_3 \rightarrow Me(AlH_4)_2/ Me(AlH_4)_3 + 2/3LiCl/NaCl$
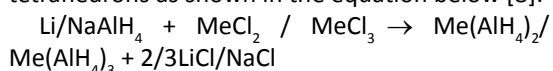
These hydrides are made of $AlH_4$ tetrahedrons connected via six or four coordinated metal atoms in a distorted octahedrals, making crystals in teragonal and monoclinic space groups.

The dehydrogenation of these $MeAlH_4$ structures usually leads to the formation of $Me_3AlH_6$ or $MeAlH_5$ compounds [2]. These intermediate structures are built of $[AlH_6]^{3-}$ or $[AlH_5]^{2-}$ units as isolated or linked in chains parts with multiple decomposition steps. These alkaline earth alanates were mostly synthesized from direct milling of aluminum, magnesium, and calcium hydrides [13]. A new prospect of alanate utilization can be based on their ability to provide fresh and ionic aluminum and alkaline earth ions with active hydrogen ions during decomposition. This group of ions can participate in any reaction, like oxidation, at low temperatures of dehydrogenation. Presence of hydrogen atoms near the reaction site during dehydrogenation can ensure targeted reactions between precursors. Also, most probable reaction can be between oxygen atoms from reaction atmosphere or outer layer oxides around precursor particles which can easily be removed from the reaction medium [14-16]. Recent studies on hydrogenation of metals (Zr, Mg-MgH$_2$ systems) and non-organic compounds (*i.e* ZrCl$_4$) with alkaline metal hydrides meta synthesis and doping shows promising processes for hydride formations [17-19].

The main aim of this study was to characterize the crystal structure and thermal behavior of alkaline earth (Mg and Ca) alanates in order to indicate the effect of alkaline earth metals content on phase transformation and thermal properties of alanates. The hydrogen desorption performance, like the hydrogen release amount and temperature, were studied by structural, thermal, and chemical analysis methods.

## EXPERIMENTAL

Magnesium and Calcium anhydrous chlorides ($MgCl_2$ and $CaCl_2$, over 98% pure, Merck, Germany) were used as alkaline earth metal precursors. Lithium aluminum hydride ($LiAlH_4$, 99% pure, Merck, Germany) and ($AlCl_3$, 97% pure, Merck, Germany) supplied the required atomic hydrogen and additional aluminum for mechano-chemical activation process. 0.1 atomic weight ratio step of alkaline earthmetal from 0.9 : 0.1 to 0.1 : 0.9 (Aluminum : Alkaline Earthmetal) molar percent was chosen for concise study of the complex hydride formations. A summarized version of the main reaction used for studying the effect of atomic weight ratio of the precursors, based on the reaction of formation of alane, is as follows:

$(AlCl_3 : MeCl_2) + 3LiAlH_4 \rightarrow$ Hydride/Alanates + $3LiCl$ + Residual/By-product phases.
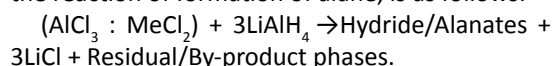
which involves the exchange of chloride and hydride bonds between lithium and alkaline earth metals, known as salt metathesis double replacement reactions [5] via mechano-chemical activation process. Additional 0.05 atomic weight ratio of Lithium chloride (LiCl, 99% pure, Merck, Germany) was also added as buffer material to assist reaction promotion. All chlorides were heated in 99.999% pure argon atmosphere at 175 °C for 6 hours in tube furnace for complete dehumidifying and drying. All handling and storing of precursors and products were carried out in a custom made glove box under $10^{-3}$ bar vacuum and high purity dry argon gas to inhibit air/moisture exposures. Different atomic weight ratio batches of precursors were loaded to a custom made hardened chromium steel vial with 500 $^{cc}$ volume. Vial head had two special valves for vacuum and gas purging with special made o-ring seals. Same $10^{-3}$ bar vacuuming for 30 min and argon 75 hydrogen 25 gas purging up to 2 bar regime was carried out for all samples. The vial was evacuated and purged for four times before milling process. Combinations of three hardened Cr - steel balls of diameters 5, 10 and 30 mm were used to supply 20:1 ball to powder weight ratio (BPR).

The mixture was milled in Fritsch pulverisette 6 (Fritsch company, Germany) high energy mono vial planetary ball mill for 3 hours at rotation speed of 300 rpm. Vial was filled up to 50% volume by precursors in each study. Extreme high energy contacts between ball, powder, and walls of vial during milling process, induced physical contacts for process activation and compounds formations. These contacts caused solid state atom/ion displacements between precursors, blending the reactants, forming nanoscale chemical mixtures, with increasing reaction kinetics [5], synthesized nano-sized products with chloride based byproducts. Removing chloride byproducts and residual precursors were carried out using nithromethane ($CH_3NO_2$) based washing stages. Four washing stages were as followed: three times washing by nitemethane: $AlCl_3$= 95 : 5 solutions and one stage with pure nitromethane which was found to be the most successful washing process. All solving, draining, and solvent evaporations were carried out in glove box. Solving processes were followed by centrifugation for 30 min in rotation speed of 2000 rpm in argon purged sample containers using Ferria 350 lab centrifuge.

The phase structure of samples were checked by XRD analysis using Philips MPD-XPERT mono chromate $Cu_{k\alpha}$ = 0.154 nm at voltage of 46 kv and 8 mA current. The scan range was between 2θ = 10° to 90° and the scan rate was 1° per min at the step size of 0.02°. Diffraction angles were reported based on best fitting range. Nanograin/Crystallite sizes were calculated based on peak broadening using Cauchy / Gaussian approximation by linear regression plot by equation [8]:

$$\frac{\delta^2(2\theta)}{\tan^2(\theta)} = \frac{k\lambda}{D}\left[\frac{\delta(2\theta)}{\tan(\theta)\sin(\theta)}\right] + 16\varepsilon^2 \quad \text{and} \quad \delta(2\theta) = B\left[1 - \left(\frac{b^2}{B^2}\right)\right]$$

The term δ(2θ) indicates instrumental-broadening correction where Kλ/D is the slope and D is the mean crystallite (nanograin) size. K is a constant about 1 and indicates the accumulated strain in the structure. Term θ is the position of the analyzed peak. B and b are the breadth of same peak (the full widths at half maximum, FWHM) of experimental and reference crystal, both in radians, respectively. Lattice parameters of phases were calculated using d spacing from bragg equation and related lattice equations [2]. The diffraction data was also used for structural refinement studies via rietveld structural refinement method [20] to calculate the extent of

agreement between observation and the model for alane phase via the residual factor ($R_p$), weight residual factor ($R_{wp}$) and S index ($R_{wp}$/ $R_{exp}$), where $R_{exp}$ is the expected $R_{wp}$ value. The initial structural parameters of alane phase were taken from the standard structure for rietveld model calculations and calculated using Philips x'pert plus for crystallography and rietveld analysis. Products were studied by XRD after milling process and after residual precursors and by products removal by washing process. Fourier transmittance infrared spectroscopy (FTIR) was captured for all samples after washing to study chemical bond types in samples and their dependency to original milled mixture contents, using Thermo-mattsen IR310, in the range of 350 to 4000 cm$^{-1}$. Differential scanning calorimetry (DSC) was performed using Netzsch404 instrument. About 15mg of samples were heated in an alumina crucible at the scan rate of 2, 5 and 10 ̊C/min under Ar production flow for reaction (dissociation) to take place at temperatures of samples. Thermo-gravimetric analysis (TGA) was performed using STA 1460 equipment instrument with15mg samples heated at a heating rate of 10 °C/min under nitrogen flow for measuring the amount of hydrogen release in samples, during heating cycle.

Morphology of powders was observed using scanning electron microscopy (Philips, XL30 series) with an accelerating voltage of 10–15 kV. Particle size observations were carried out by FE-SEM (Hitachi, 501xr) at accelerating voltage of 15.0-17.0 kV.

## RESULTS AND DISCUSSION
### Magnesium: Aluminum

We chose a 0.1 atomic weight ratio step of alkaline earth metal from 0.9 : 0.1 to 0.1 : 0.9 (aluminum: alkaline earth metal) to study the MCA process progression and different products formation. The XRD patterns of 0.1 to 0.9 of magnesium atomic weight ratio mixture samples milled at rotating speed of 300 rpm for 3 h with ball to powder weight ratio of 20:1 under Ar-$H_2$ atmosphere and washed Al : Mg = 0.1 : 0.9 sample are shown in Fig. 1 (a – j). The decrease in relative peak intensities of starting precursors like $AlCl_3$ and $MgCl_2$ indicated the proceeding of reactions via mechano-chemical activation process. Two known reactions could control the chemical bonds changes during mechanical milling [7]:

$3LiAlH_4 + AlCl_3 \rightarrow 4AlH_3 + 3LiCl$
$2LiAlH_4 + MgCl_2 \rightarrow Mg(AlH_4)_2 + 2LiCl$
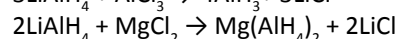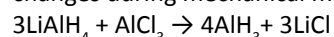
As seen, there are no sign of LiAlH$_4$ characteristic peaks in any samples, which indicates complete participation of hydrogen source precursors in the reactions. The presence of the basic hydrides and alanates diffraction peaks in all milling mixtures and no sign of crystallized metal or alloys diffraction peaks can indicate a very small amount of dehydrogenation during the milling processes in all precursors' atomic weight ratios. Mechano-chemically activated phases can be categorized in three groups. First, residual or non-participant precursors like AlCl$_3$ and MgCl$_2$ which might not have reacted with other precursors because of the non-stoichiometric nature of the process or even might have been formed by reverse reactions during milling. Second group are hydrides or alanates formed based on the presence of enough ions to promote reactions for AlH$_3$ or Mg(AlH$_4$)$_2$ formation. Third group are buffer chemicals and reaction byproducts like LiCl which can be seen in all patterns with high intensity peaks. Small amount of chlorine evolution was detected based on the smell during opening of vial after milling which can be caused by dissociation of precursors. No diffraction peaks for metallic lithium, aluminum, or alkaline earth metals were detected in as-milled samples. Small amount of residual lithium, due to non-equilibrium and non-stoichiometric nature of the process, is possible. The formation of amorphous chloride phases was unlikely due to the nature of these materials and fast dissociation during early stages of milling. Alane is the main hydride phase in samples from Al : Mg = 0.9 : 0.1 up to 0.5 : 0.5 atomic weight ratios. Residual and non-participant MgCl$_2$ are seen in 0.2 : 0.8 and 0.3 : 0.7 molar ratio samples. Small reacting affinity and lower activity of magnesium could cause residual magnesium chloride in the mixtures. Magnesium based hydrides/alanates were first detected in 0.4 : 0.6 atomic weight ratio with small amount of residual aluminum chloride in the mixtures. Participation of magnesium chloride was indicated by the decrease in peak intensities at 0.4 : 0.6 and 0.5 : 0.5 atomic weight ratios with presence of aluminum chloride as a result of non-proceeding reaction of alane formation. At 0.5:0.5 atomic weight ratios, leading reaction changed and magnesium alanate was formed as the main hydride phase. Small quantities of alane were detected up to 0.3 : 0.7 atomic weight ratios samples. Aluminum chloride characteristic peaks disappeared in samples 0.3 : 0.7 to 0.1 : 0.9, which

coincided with complete utilization of aluminum during Mg(AlH$_4$)$_2$ formation. Small amount of aluminum hydride was formed in 0.4 : 0.6 and 0.3 : 0.7samples which can be caused by the change in the leading reaction during the milling process. Mg(AlH$_4$)$_2$was the main structure in 0.3 : 0.7 to 0.1 : 0.9 atomic weight ratios samples with small amount of residual magnesium chloride. Diffraction pattern of the washed 0.1 : 0.9 atomic weight ratio sample is shown in Fig. 1j. The pattern had no diffraction peaks of residual or by-product materials which indicate the efficiency of the washing process. All samples were washed before collecting diffraction data for measuring lattice structure parameters and crystallite sizes reported at Table 1. Alane is the main phase from 0.9:0.1 up to 0.7:0.3 atomic weight ratio of Al : Mg. which was crystallized in centered rhombohedral crystal structure in a good agreement with α alane phase. Slight increase in α and c lattice parameters were calculated by increasing the magnesium content in milled mixtures. This increase was mostly caused by interstitial doping of magnesium ions into alane structure which expanded the unit cell, mostly in basal parameters. Continuous increase in both base and height lattice parameters, until the formation of magnesium alanate phase, shows homogeneous doping of magnesium into aluminum hydride structure. These changes caused an increase in unit cell volume up to 1.47% relative to standard pattern lattice volume. By formation of Mg(AlH$_4$)$_2$ phase around 0.5 : 0.5 atomic weight ratio of Al : Mg, changes in alane lattice structures stopped and even decreased to original lattice parameters which can be related to the end of Mg doping into alane crystal structure. Magnesium alanate was formed in tetragonal (HCP) crystal structure with lattice parameters about 5.200 Å (a) and 5.860 Å (c). Mg(AlH$_4$)$_2$ structures showed non growing tetragonal crystals normal to the basal plants. Changes in lattice parameters in magnesium alanates was a slight decrease in lattice parameters α and c, resulting in unit cell shrinkage up to 0.36%. These changes were small in regard to alane phase, indicating no apparent change in crystal structure caused by solid solution or doping. Calculated crystallite sizes, using peak broadening (FWHM) and Cauchy / Gaussian approximation formula, indicated the formation of particles with 10 to 20 nm crystallites. R-values for rietveld structural refinement of samples with doped alane phase

are reported in Table 2. Acceptable quality of refinement was achieved based on the low values of $R_{wp}$, indicating good adjustment between observed and calculated data, and relatively good fitness of the results based on S values. As seen, the $R_p$ values are slightly high which indicates the low crystallinity of the acquired diffraction data compared to the standard model. Considering the sharp diffraction peaks of alane phase and low background in the patterns, this can be caused by special atomic order due to the presence of doped magnesium in alane phase structure. Small range disorder, especially in (014) planes was calculated which can indicate a modified alane structure. As seen, highest $R_p$ values are calculated for samples with most unit cell volume change due to doping magnesium in alane structure. Samples elemental bonds were also checked using infra-red transmittance analysis. FTIR patterns of different Al : Mg atomic weight ratios washed samples are shown in Fig. 2. There are two sets of broad band peaks in the samples. Wave lengths about 642 and 1875 cm$^{-1}$, belonged to $Mg(AlH_4)_2$ and near 1675 and 738 cm$^{-1}$ for Al-H bonds in $AlH_3$ structures [1]. Increasing Mg content in initial precursor's mixture from 0.1 to 0.9 atomic weight ratios caused more vivid transmittance valleys in patterns regarding to $Mg(AlH_4)_2$. From Al : Mg=0.6

: 0.4 up to 0.3 : 0.7, characteristic wave lengths for both structures were present, which is in a good conformity with XRD results, indicating formation of mixtures of both structures in washed samples. These samples have patterns with different characteristic FTIR peaks which can be related to formation of various bonds between aluminum/magnesium and hydrogen atoms. As seen, samples with Al : Mg=0.9 : 0.1 and 0.1 : 0.9 atomic weight ratios showed strong patterns of pure $AlH_3$ and $Mg(AlH_4)_2$, respectively. These results clearly show that $Mg(AlH_4)_2$ and $AlH_3$ or controlled mixtures of them could be prepared by the mechano-chemical reaction between earth metal chlorides and lithium alanate.

Alane and alanates are mostly unstable (thermodynamically) in a large temperature range but their decomposition is kinetically limited. With constant increase of temperature, hydrides/alanates decompose with considerable thermal energy absorption/desorption (endothermic/exothermic). In order to indicate thermal behavior (dissociation temperatures) and hydrogen release with increasing the magnesium content, samples were studied by differential scanning calorimetry (DSC) and thermo-gravimetric analysis (TGA). DSC results were used to study the thermodynamics of the hydrogen release like dissociation
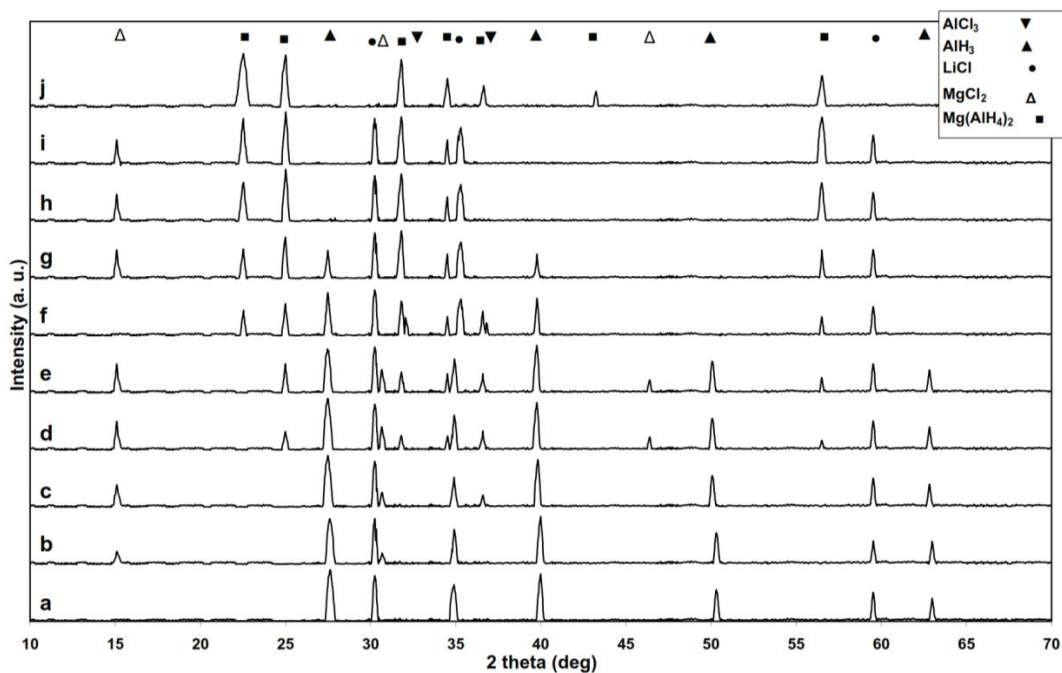


Fig. 1: XRD patterns for 0.1 to 0.9 magnesium atomic weight ratio (a to i) and 0.1 : 0.9= Al :Mg washed sample (j).

temperature, steps, and the activation energy for decomposition of hydrides / alanates. Activation energies were calculated using Kissinger relation,

$$\left(\frac{C}{T_p^2}\right) \propto -\frac{E_a}{RT_p}$$

where by drawing different heating rates (C) over square of peak temperatures (Tp) versus , the activation energies (Ea) can be measured as the slope of the plots. Normal DSC and TGA patterns at heating rate of 10 °C / min for different atomic weight ratios of Al : Mg washed samples are shown in Fig. 3.

Samples with single alane phase (Al : Mg= 0.9 : 0.1 up to 0.6 : 0.4) showed only one endothermic peak related to hydrogen dissociation of AlH$_3$. Dissociation temperature was near 150 °C, which decreases to near 147 °C with more magnesium contents up to 0.6. As seen, patterns showed different shape and peak intensities with non similar ascending and descending slopes. These

behaviors are mostly related to formation of new bonds in the structures regarding to Al-H and Al-H-Mg presence in the structure. This phenomenon cannot be easily detected by phase study via XRD or bond study in FTIR analysis due to the low contents, mostly under test method resolutions. By formation of independent phases like magnesium alanates in Al : Mg=0.7 : 0.3 up to 0.1 : 0.9 samples, characteristic peaks in different temperatures and even exothermic peaks were revealed. Exothermic peaks at 130 to 140 °C and endothermic peaks with wide formation ranges near 265 to 280 °C are attributed to the two step response of magnesium alanate to one stage heating cycle [3]. These peaks continued to fade near 150 °C endothermic peak of alane and in Al : Mg=0.1 : 0.9 only strong peaks of Mg(AlH$_4$)$_2$ were detected. As seen, the exothermic peak (near 130 °C) became sharper during structure change with an endothermic peak which could be easily detected at 285 °C. Hydrogen contents of

Table (1): Crystal Structure, lattice parameters, lattice volume, lattice volume change percent, and calculated crystallite size of milled and washed samples with 0.1 to 0.9 molar ratio of Mg.

| Sample (Al:Mg) | Phase | Crystal Structure | Lattice parameters(Å) ±0.001 | Δα/α$_0$ (%) Δc/c$_0$ (%)* | Lattice Volume(Å$^3$) ±0.0001 | Δv/v$_0$ (%)* | Crystallite size (nm) |
|---|---|---|---|---|---|---|---|
| 0.9:0.1 | AlH$_3$ | Rhombohedral | a=b=4.450 | 0.02 | 202.4435 | 0.06 | 10 |
|  |  |  | c=11.805 | 0.02 |  |  |  |
| 0.8:0.2 | AlH$_3$ | Rhombohedral | a=b=4.459 | 0.22 | 203.3665 | 0.52 | 19 |
|  |  |  | c=11.811 | 0.07 |  |  |  |
| 0.7:0.3 | AlH$_3$ | Rhombohedral | a=b=4.467 | 0.40 | 204.3734 | 1.02 | 12 |
|  |  |  | c=11.827 | 0.20 |  |  |  |
| 0.6:0.4 | AlH$_3$ | Rhombohedral | a=b=4.476 | 0.61 | 205.3019 | 1.47 | 15 |
|  |  |  | c=11.833 | 0.25 |  |  |  |
|  | Mg(AlH$_4$)$_2$ | Trigonal | a=b=5.191 | -0.15 | 136.6302 | -0.36 | 17 |
|  |  |  | c=5.855 | -0.05 |  |  |  |
| 0.5:0.5 | AlH$_3$ | Rhombohedral | a=b=4.473 | 0.54 | 204.9401 | 1.30 | 15 |
|  |  |  | c=11.828 | 0.21 |  |  |  |
|  | Mg(AlH$_4$)$_2$ | Trigonal | a=b=5.193 | -0.12 | 136.8757 | -0.18 | 13 |
|  |  |  | c=5.861 | 0.05 |  |  |  |
| 0.4:0.6 | AlH$_3$ | Rhombohedral | a=b=4.477 | 0.63 | 205.2027 | 1.43 | 13 |
|  |  |  | c=11.822 | 0.16 |  |  |  |
|  | Mg(AlH$_4$)$_2$ | Trigonal | a=b=5.195 | -0.08 | 136.911 | -0.15 | 16 |
|  |  |  | c=5.858 | 0.00 |  |  |  |
| 0.3:0.7 | AlH$_3$ | Rhombohedral | a=b=4.472 | 0.52 | 204.7446 | 1.20 | 12 |
|  |  |  | c=11.822 | 0.16 |  |  |  |
|  | Mg(AlH$_4$)$_2$ | Trigonal | a=b=5.195 | -0.08 | 136.911 | -0.15 | 18 |
|  |  |  | c=5.858 | 0.00 |  |  |  |
| 0.2:0.8 | Mg(AlH$_4$)$_2$ | Trigonal | a=b=5.196 | -0.06 | 136.9637 | -0.12 | 15 |
|  |  |  | c=5.858 | 0.00 |  |  |  |
| 0.1:0.9 | Mg(AlH$_4$)$_2$ | Trigonal | a=b=5.199 | 0.00 | 137.1219 | 0.00 | 9 |
|  |  |  | c=5.858 | 0.00 |  |  |  |

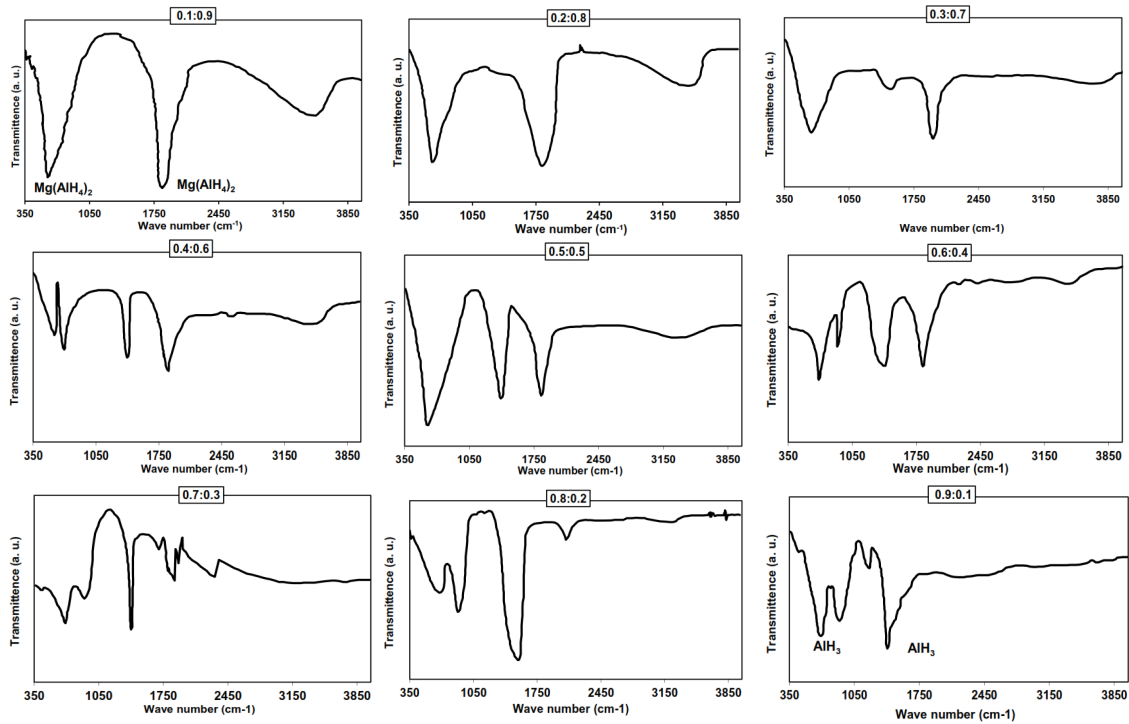*regarding to standard pattern lattice parameters

Fig. 2: FTIR spectra for Al:Mg samples from 0.1 : 0.9 to 0.9 : 0.1 atomic weight ratios.

Table 2: Rietveld refinement indexes for structures with doped alane phase in Al:Mg system.

| Sample (Al:Mg) | $R_{wp}$ | S | $R_p$ |
|---|---|---|---|
| 0.9:0.1 | 4.08 | 1.10 | 19.11 |
| 0.8:0.2 | 4.12 | 1.13 | 19.38 |
| 0.7:0.3 | 4.17 | 1.12 | 20.24 |
| 0.6:0.4 | 4.23 | 1.17 | 29.73 |
| 0.5:0.5 | 4.14 | 1.12 | 25.02 |
| 0.4:0.6 | 4.21 | 1.13 | 26.81 |
| 0.3:0.7 | 4.12 | 1.15 | 21.63 |

hydrides can be calculated via TGA patterns. Fig. 3 also shows TGA patterns of samples in a close weight change range of 100 to 90%. It should be noted that due to the solid based process of formation (mechano-chemical activation process) and extremely volatile nature of washing medium, no external impurity or organic based material was expected which was confirmed by no sign of chemical release/dissociation in the DSC and TGA results. Samples showed one step weight loss (hydrogen dissociation) up to ~ 8wt% near 150 °C in alane phase samples. Second dissociation (weight loss) steps slowly formed by increasing magnesium content, which changed from the one step hydrogen release of alane phase to a 7.5wt% at 147 °C and 1.6wt% at 169 °C two step dissociation for A l: Mg=0.5 : 0.5 sample. Dissociation temperatures changed to 140 °C with 5.5wt% and 275 °C with ~2.1wt% weight loss in Al : Mg=0.3 : 0.7 atomic weight ratio. Atomic weight ratios of Al : Mg=0.2 : 0.8 and 0.1 : 0.9 clearly showed the two step dissociation behavior of magnesium alanates with total hydrogen content of ~9.2 wt%. Most probable hydrogen release equations are shown as onset in Al : Mg=0.9 : 0.1 and 0.1 : 0.9 curves. Table 3 shows calculated hydrogen dissociation activation energies for samples using three heating rates and kissinger plots. Calculated values are

the combination of exothermic and endothermic behavior of aluminum hydride and magnesium alanate, respectively. It shows the accumulated amount of activation energy necessary for hydrogen release from the samples. $AlH_3$ based samples required near 80 kj/mol activation energy to start releasing hydrogen while magnesium alanate absorbed near 64 kj/mol. Forming hydride mixtures of both hydride and alanate phases caused considerable heat absorption for hydrogen dissociation. It increased upto 152 kj/molin 0.5 : 0.5 atomic weight ratio mixture in two step dissociation of aluminum hydride and magnesium alanate, respectively. Higher amount of activation energy necessary for mixture dissociation in 0.5 : 0.5 atomic weight ratio can be caused by the presence of both hydride and alanate in this sample, which required more activation energy to start dissociation.

The studies were continued on heating process products, with same procedure used in DSC and TGA evaluation, to indicate the most probable products of hydride dissociation. Besides studying the effect of composition on hydrogen release of
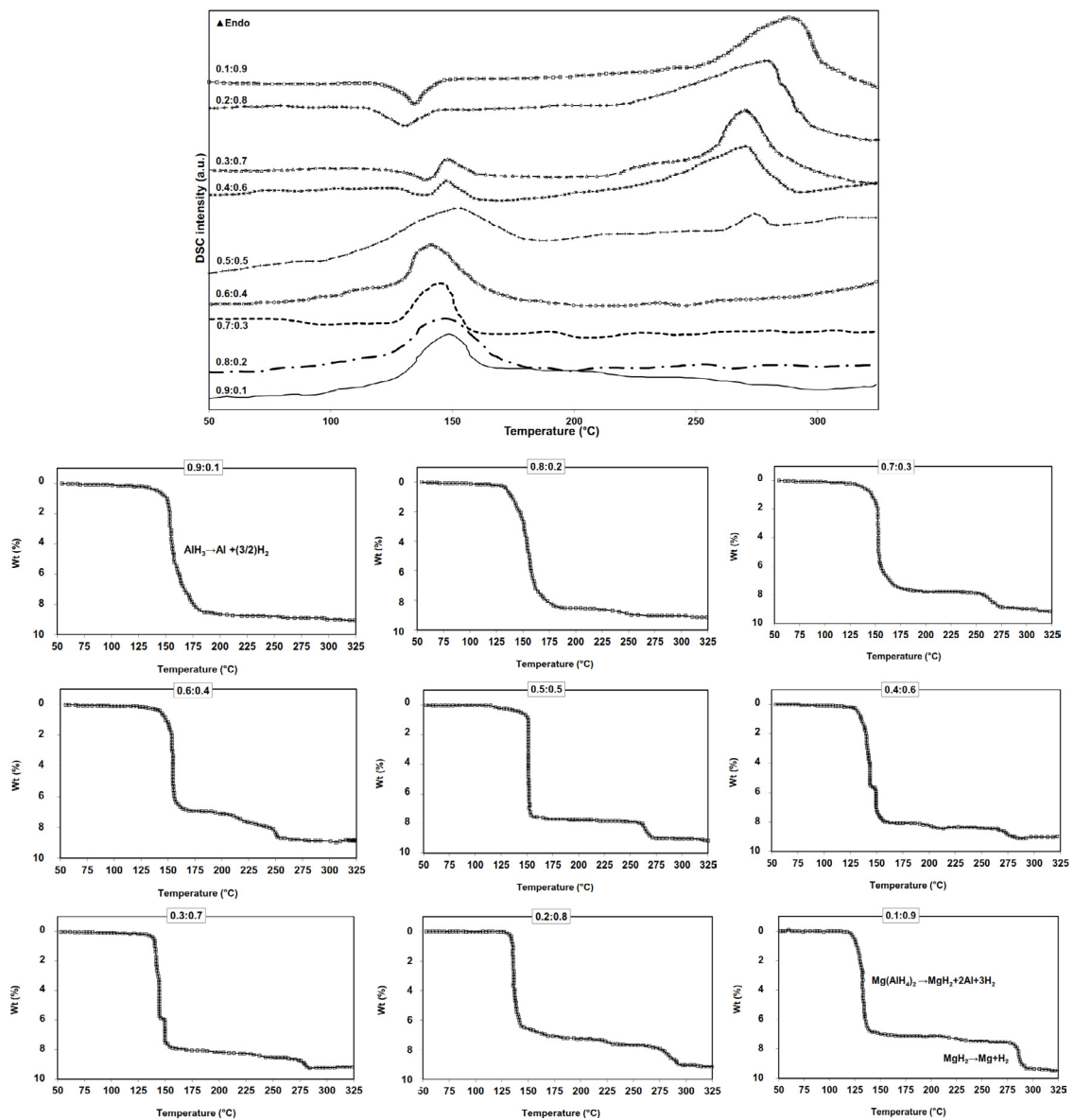


Fig. 3: DSC and TGA patterns of Al : Mg samples from 0.9 : 0.1 to 0.1 : 0.9 atomic weight ratios.

Table 3: Dissociation activation energy for washed samples
with 0.1 to 0.9 molar ratio of Mg.

| Sample (Al:Mg) | Activation energies (Ea) |
|---|---|
| 0.9:0.1 | 83 KJ/mol |
| 0.8:0.2 | 81 KJ/mol |
| 0.7:0.3 | 80 KJ/mol |
| 0.6:0.4 | 123 KJ/mol |
| 0.5:0.5 | 152 KJ/mol |
| 0.4:0.6 | 145 KJ/mol |
| 0.3:0.7 | 136 KJ/mol |
| 0.2:0.8 | 63 KJ/mol |
| 0.1:0.9 | 64 KJ/mol |

hydrides/alanates in Al-Mg system, these mixtures can be considered as suitable delivery system for pure/alloyed nano-sized metal particles. In-situ formation of these materials via a low temperature one step heating process, nevertheless in the safe medium made by hydrogen release, can be very interesting. The residual materials after heating at the speed of 10 °C /min in argon atmosphere and cooled under vacuum and high purity argon purged medium were analyzed by XRD shortly after dissociation. Diffraction patterns are shown in Fig. 4 for all samples. As seen, No characteristic peaks for aluminum, magnesium, or their complex oxides were detected in any sample. Due to small bond length of Al-H and Mg-H-Al in hydride and alanate phases, the heated samples were mostly alloyed Al with magnesium, alloyed Mg with aluminum, and magnesium – aluminum intermetallics with large cubic unit cells. Increasing magnesium content from 0.1 to 0.3 atomic weight ratios caused formation of aluminum phase with diffraction peaks slightly moved to lower diffraction angles after heating. Higher amount of magnesium, especially 0.4 to 0.6 atomic weight ratios, enhanced formation of Mg-Al intermetallic phases like $Mg_2Al_3$ and in higher contents $Mg_{17}Al_{12}$ with FCC and BCC crystal systems, respectively. Magnesium contents from 0.7 to 0.9, caused formation of magnesium as the remaining phase. Alloying with aluminum moved the Mg (HCP) characteristic peaks up to higher values. Detailed properties of remaining metals and alloys are mentioned in Table 4. Alloying aluminum with residual magnesium after heating can be concluded from increases in Al unit cell

parameters and unit cell volume by entering large Mg atoms into Al structure in 0.9 : 0.1 to 0.7 : 0.3 samples. On contrary, interstitial entrance of aluminum into magnesium structure in 0.3 : 0.7 to 0.1 : 0.9 samples caused unit cell contraction in magnesium alloyed phases. Stoichiometric intermetallics phases were seen in 0.6 : 0.4 to 0.4 : 0.6 samples. Additional calculations indicated that these phases were formed by 6 to 12 nm crystallites, as mentioned in the last column of the Table 4.

FE-SEM studies of samples showed agglomerated nano sized samples with irregular shapes, which is the expected morphology from mechano-chemical activation process. Micrographs of Al : Mg=0.9 : 0.1 and 0.1 : 0.9 are shown in Fig. 4a and 4b as an example of typical morphology of synthesized hydride and alanates and their shape after heating Fig. 4c,d. As seen, even at high resolutions, particle borders are hard to indicate. It seems that particle sizes were near 20-30 nm in hydride and alanate and slightly increased to about 50-60 nm for alloyed samples.

*Calcium: Aluminum*

Same 0.1 atomic weight ratio step of calcium content was chosen for 0.9 : 0.1 to 0.1 : 0.9 Al : Ca atomic weight ratio samples. The XRD patterns of 0.1 to 0.9 calcium atomic weight ratio mixture samples milled at rotating speed of 300 rpm for 3 h with ball to powder weight ratio of 20 : 1 under Ar-$H_2$ atmosphere and washed Al : Ca = 0.1 : 0.9 sample are shown in Fig. 5 (a-j). Samples showed different alane and alanates formation behavior from Al:Mg samples. As seen, main phases were $AlH_3$ and $Ca(AlH_4)_2$ in low and high calcium contents, respectively. By increasing Ca atomic weight ratios in samples, main hydride phase changed slowly from aluminum hydride to calcium alanates near 0.5 : 0.5 atomic weight ratios and continued to be the main phase in the 0.1 : 0.9 washed sample (Fig. 5j). $Ca(AlH_4)_2$ is made by central calcium ion occupying a crystallographic octahedrally coordinated by two hydrogen atoms of two $[AlH_4]$ units, with monoclinic and $P_{21}/n$ space group. Proceeding inalanates formation can be detected via the decrease in characteristic peaks of $LiAlH_4$, $AlCl_3$ and $CaCl_2$ precursor's in diffraction patterns. Calcium and aluminum chloride characteristic peaks were detected in all patterns which could be related to non-completed formation reactions like:
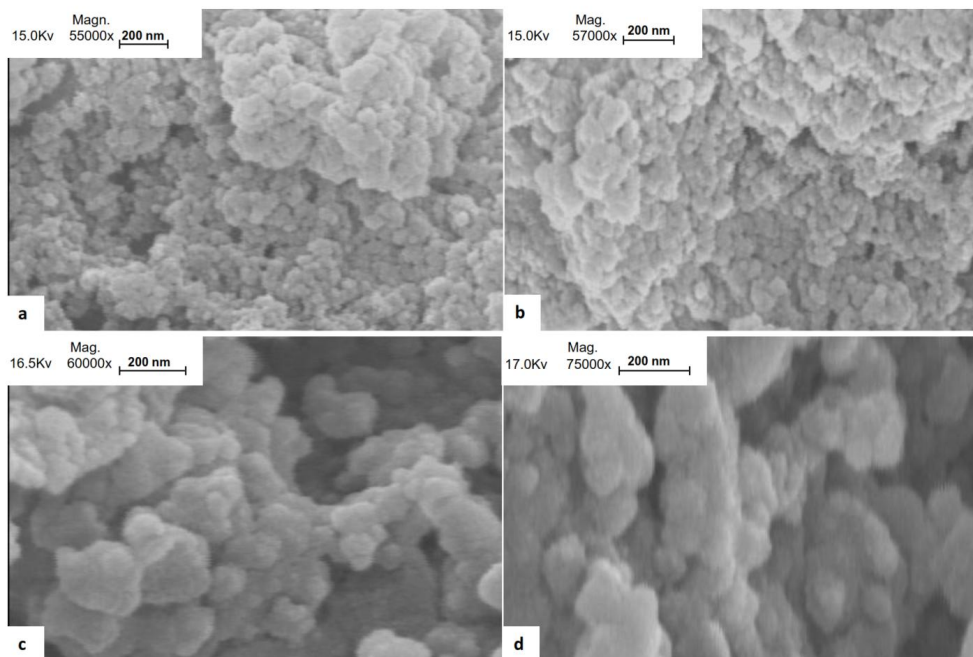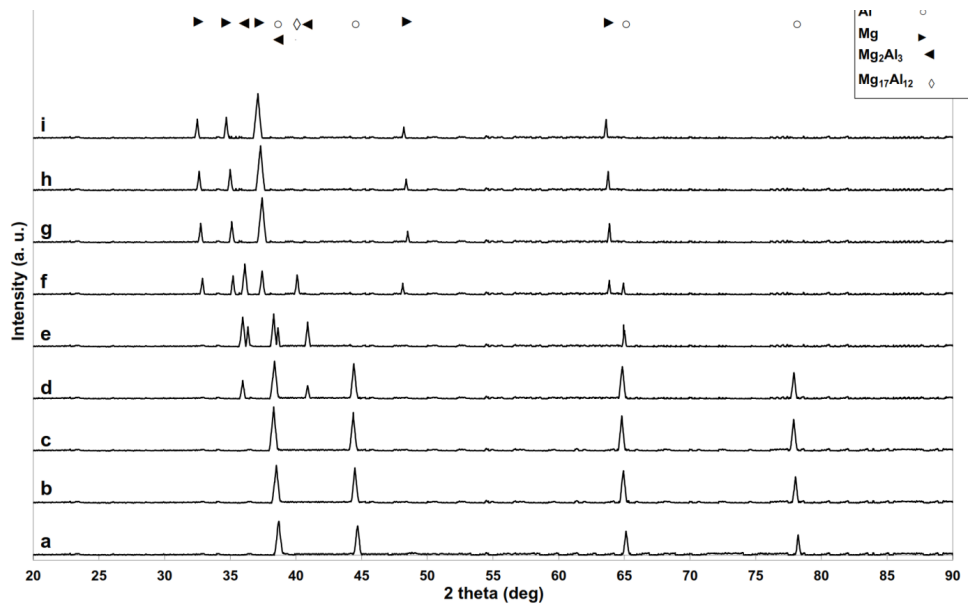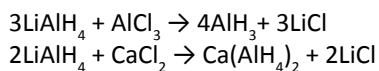
Fig. 4: XRD patterns of heated 0.1 to 0.9 magnesium atomic weight ratio (a to i) samples and FE-SEM micrographs of Al:Mg=0.9 : 0.1 and 0.1: 0.9 samples after washing process (a,b) and after heating process (c,d).

$$3LiAlH_4 + AlCl_3 \rightarrow 4AlH_3 + 3LiCl$$
$$2LiAlH_4 + CaCl_2 \rightarrow Ca(AlH_4)_2 + 2LiCl$$

It seemed that despite the fact that Ca and Mg are next to each other in the alkaline earth column of periodic table, Mg showed higher tendency for participation in hydride formation which could lead to dissociation of precursors, while calcium only tends to change corner connected $AlH_6$ octahedra with each H bridging two octahedral of alane to interconnected $[AlH_4]$ tetrahedrons with Ca ion in the middle. The residual or none participant precursors might have refused to react with other precursors because of the non-stoichiometric nature of the process or even might have been formed by reversed reactions during milling activation process. Signs of alanate formation were first seen in 0.7 : 0.3 and 0.6 : 0.4 atomic weight ratios which were accompanied by low

Table 4: Crystal Structure, lattice parameters, lattice volume, lattice volume change percent, and calculated crystallite size of heated and samples with 0.1 to 0.9 molar ratio of Mg.

| Sample (Al:Mg) | Phase | Crystal Structure | Lattice parameters(Å) ±0.001 | $\Delta\alpha/\alpha_0$ (%) * | Lattice Volume(Å³) ±0.0001 | $\Delta v/v_0$ (%)* | Crystallite size (nm) |
|---|---|---|---|---|---|---|---|
| 0.9:0.1 | Al | FCC | a= 4.08 | 0.77 | 67.92 | 0.02 | 9 |
| 0.8:0.2 | Al | FCC | a=4.12 | 1.75 | 69.93 | 0.05 | 7 |
| 0.7:0.3 | Al | FCC | a= 4.19 | 3.5 | 73.56 | 0.11 | 10 |
| 0.6:0.4 | Al | FCC | a= 4.14 | 2.25 | 70.96 | 0.07 | 8 |
|  | Mg₂Al₃ | FCC | a= 28.24 | 0.04 | 22521 | 0.001 | 12 |
| 0.5:0.5 | Al | FCC | a= 4.13 | 2 | 70.45 | 0.06 | 6 |
|  | Mg₂Al₃ | FCC | a= 28.25 | 0.07 | 22545 | 0.002 | 11 |
| 0.4:0.6 | Mg | HCP | a= 3.200 / c=5.210 | -0.3 / -0.02 | 46.201446 | -0.006 | 7 |
|  | Mg₁₇Al₁₂ | BCC | a= 10.55 | 0.09 | 1174 | 0.003 | 12 |
| 0.3:0.7 | Mg | HCP | a=3.114 / c=5.196 | -3 / -0.30 | 43.61 | -0.06 | 9 |
| 0.2:0.8 | Mg | HCP | a=3.118 / c=5.200 | -2.84 / -0.21 | 43.78 | -0.05 | 11 |
| 0.1:0.9 | Mg | HCP | a=3.119 / c=5.209 | -2.80 / -0.04 | 43.88 | -0.05 | 12 |

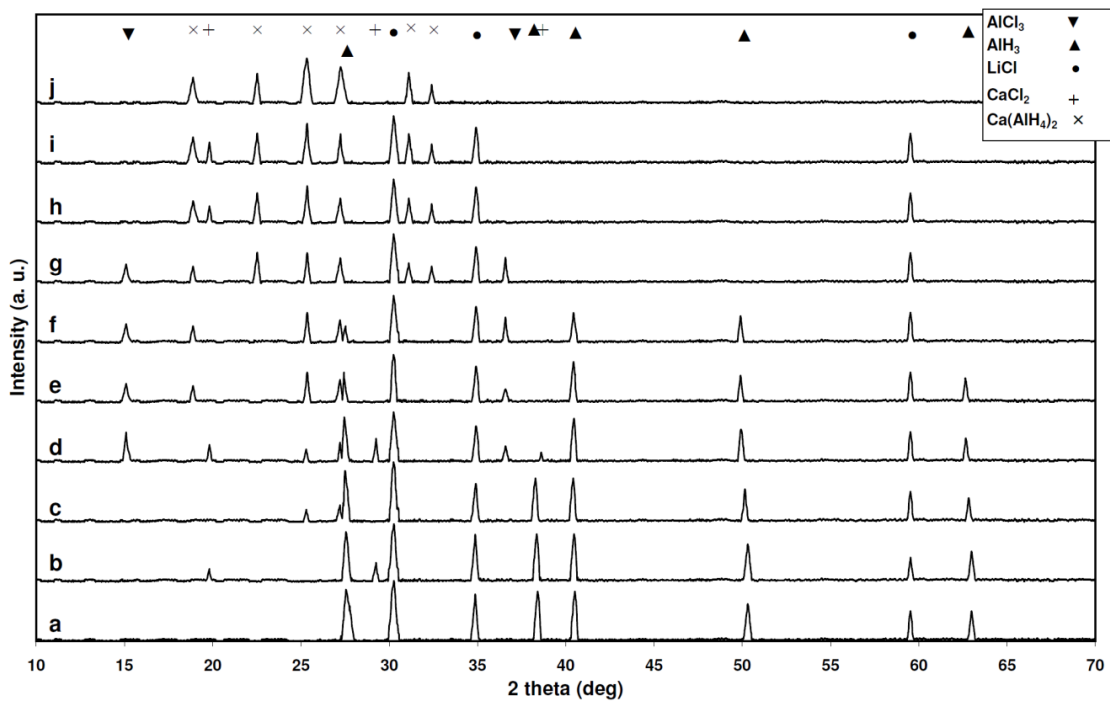* regarding to standard pattern lattice parameters



Fig. 5: XRD patterns for 0.1 to 0.9 calcium atomic weight ratio (a to i) and 0.1 : 0.9= Al: Ca washed sample (j).

intensity peaks of aluminum chloride. Increasing calcium in 0.4 : 0.6 to 0.1 : 0.9 atomic weight ratios samples caused complete participation of aluminum chloride with more non-participant calcium chlorides. No characteristic diffraction peaks of other calcium hydride or alanates like $CaH_2$ and $CaAlH_5$ were detected which suggests a one step alanate formation in these samples.

Calculated crystal structure parameters of the washed samples are reported in Table 5. Alane with rhombohedral and calcium alanate with monoclinic crystal structure were the main phases. Small increases in unit cell volume of alane phases up to 1.54% in 0.5 : 0.5 atomic weight ratio, caused by increases in both basal and c-axis parameters, can be related to the small amount of calcium ion interstitial solutions. Calcium alanate showed different structure with smaller unit cells near -0.45% than predicted in 0.7 : 0.3 sample, where it was first detected, while changing to slightly larger unit cell in 0.1 : 0.9 sample. Most changes in calcium alanate happened along α and c parameters, while b parameter was almost

identical. Calculated crystallite sizes for all samples were about 20-45 nm with no apparent trend in either phases which can be attributed to the nature of mechano-chemical activation process. Table 6 shows the rietveld structural refinement values for Al : Ca samples with doped alane phase. Same low range disorder, causing less crystallinity agreement between observed and calculated data with increasing $R_p$ values with more calcium doping into alane structure, was calculated. FTIR patterns of 0.1 : 0.9 to 0.9 : 0.1 Al : Ca atomic weight ratios washed samples are shown in Fig. 6. Broad band peaks at wave lengths about 650 and 1775 $cm^{-1}$ belong to $Ca(AlH_4)_2$ and near 1675, 993 and 738 $cm^{-1}$ for Al-H bonds in $AlH_3$ structures [1,18]. Increasing calcium contents in initial precursor's mixtures from 0.1 to 0.9 atomic weight ratios caused more vivid transmittance valleys in patterns regarding to calcium alanates. Presence of characteristic wave lengths of both alane and calcium alanate phases in 0.7 : 0.3 to 0.4 : 0.6 atomic weight ratios indicated the formation of the mixture of Al-H and $[AlH_4]$-Ca-$[AlH_4]$ bonds in either phases. As seen,

Table 5: Crystal Structure, lattice parameters, lattice volume, lattice volume change percent, and calculated crystallite size of milled and washed samples with 0.1 to 0.9 molar ratio of Ca.

| Sample (Al:Ca) | Phase | Crystal Structure | Lattice parameters(Å) $\pm0.001$ | $\Delta\alpha/\alpha_0$ (%) * | Lattice Volume($Å^3$) $\pm0.0001$ | $\Delta v/v_0$ (%)* | Crystallite size (nm) |
|---|---|---|---|---|---|---|---|
| 0.9:0.1 | $AlH_3$ | Rhombohedral | a=b=4.453 | 0.09 | 202.8368 | 0.26 | 25 |
| | | | c=11.812 | 0.08 | | | |
| 0.8:0.2 | $AlH_3$ | Rhombohedral | a=b=4.462 | 0.29 | 203.7093 | 0.69 | 32 |
| | | | c=11.815 | 0.10 | | | |
| 0.7:0.3 | $AlH_3$ | Rhombohedral | a=b=4.471 | 0.49 | 204.6011 | 1.12 | 26 |
| | | | c=11.819 | 0.14 | | | |
| | $Ca(AlH_4)_2$ | Monoclinic | a= 8.365 | -0.17 | 566.5576 | -0.45 | 41 |
| | | | b=6.922 | -0.1 | | | |
| | | | c=9.806 | -0.08 | | | |
| 0.6:0.4 | $AlH_3$ | Rhombohedral | a=b=4.479 | 0.67 | 205.3861 | 1.52 | 24 |
| | | | c=11.822 | 0.16 | | | |
| | $Ca(AlH_4)_2$ | Monoclinic | a= 8.366 | -0.16 | 566.9865 | -0.37 | 22 |
| | | | b=6.925 | -0.06 | | | |
| | | | c=9.808 | -0.06 | | | |
| 0.5:0.5 | $AlH_3$ | Rhombohedral | a=b=4.479 | 0.67 | 204.6163 | 1.54 | 33 |
| | | | c=11.825 | 0.19 | | | |
| | $Ca(AlH_4)_2$ | Monoclinic | a= 8.366 | -0.16 | 567.2321 | -0.33 | 30 |
| | | | b=6.928 | -0.01 | | | |
| | | | c=9.808 | -0.06 | | | |
| 0.4:0.6 | $AlH_3$ | Rhombohedral | a=b=4.477 | 0.47 | 204.6134 | 1.13 | 25 |
| | | | c=11.825 | 0.19 | | | |
| | $Ca(AlH_4)_2$ | Monoclinic | a= 8.369 | -0.12 | 567.4943 | -0.28 | 21 |
| | | | b=6.928 | -0.01 | | | |
| | | | c=9.809 | -0.05 | | | |
| 0.3:0.7 | $Ca(AlH_4)_2$ | Monoclinic | a= 8.374 | -0.06 | 568.0302 | -0.19 | 27 |
| | | | b=6.929 | 0.00 | | | |
| | | | c=9.811 | -0.03 | | | |
| 0.2:0.8 | $Ca(AlH_4)_2$ | Monoclinic | a= 8.375 | -0.05 | 568.0980 | -0.18 | 25 |
| | | | b=6.929 | 0.00 | | | |
| | | | c=9.811 | -0.03 | | | |
| 0.1:0.9 | $Ca(AlH_4)_2$ | Monoclinic | a= 8.378 | -0.01 | 568.4753 | -0.11 | 21 |
| | | | b=6.929 | 0.00 | | | |
| | | | c=9.811 | -0.03 | | | |

* regarding to standard pattern lattice parameters

samples with Al : Ca=0.9 : 0.1 and 0.1 : 0.9 atomic weight ratios showed strong patterns of pure $AlH_3$ and $Ca(AlH_4)_2$, respectively. These results clearly show that $Ca(AlH_4)_2$ and $AlH_3$ or any controlled mixtures of them could be prepared via mechano-chemical activation process using calcium chloride and lithium alanate.

DSC and TGA patterns for all atomic weight ratios are shown in Fig. 7. Samples with alane main phase (Al : Ca=0.9 : 0.1 up to 0.8 : 0.2) showed one endothermic peak related to hydrogen dissociation at temperatures near 158 °C, which stayed identical by increasing calcium content up to 0.2. The broad endothermic peak changed to a narrower peak by each 0.1 atomic weight ratio step up to 0.4 : 0.6 sample and decreased to near 140 °C. Decrease in peak width and temperature was caused by transformation in the bonds from Al-H to Al-H-Ca-H-Al during phase changes by increasing calcium contents. Calcium alanate showed different DSC profile, with three distinguished peaks: 127 °C exothermic, 260 °C endothermic, and 328 °C endothermic peaks in the 0.1 : 0.9 sample which are caused by formation of $CaAlH_5$, $CaH_2$ and Al-Ca according to following equations [17]:
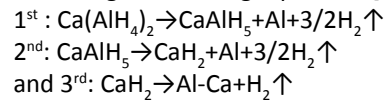
$1^{st} : Ca(AlH_4)_2 \rightarrow CaAlH_5 + Al + 3/2H_2 \uparrow$

$2^{nd}: CaAlH_5 \rightarrow CaH_2 + Al + 3/2H_2 \uparrow$

and $3^{rd}: CaH_2 \rightarrow Al\text{-}Ca + H_2 \uparrow$

Table 6: Rietveld refinement indexes for structures with doped alane phase in Al : Ca system.

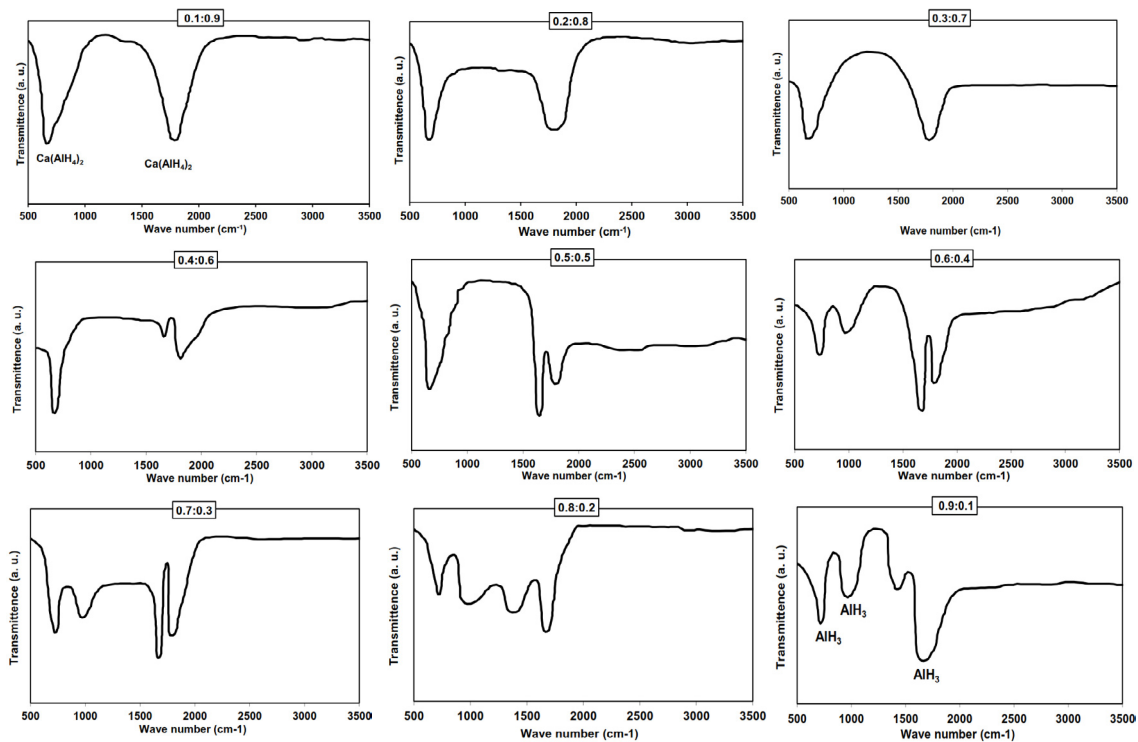| Sample (Al:Ca) | $R_{wp}$ | S | $R_p$ |
|---|---|---|---|
| 0.9:0.1 | 4.01 | 1.14 | 19.11 |
| 0.8:0.2 | 4.05 | 1.12 | 19.15 |
| 0.7:0.3 | 4.08 | 1.12 | 19.61 |
| 0.6:0.4 | 4.11 | 1.14 | 20.91 |
| 0.5:0.5 | 4.13 | 1.13 | 21.12 |
| 0.4:0.6 | 4.08 | 1.14 | 19.60 |



Fig. 6: FTIR spectra for Al:Ca samples from 0.1 : 0.9 to 0.9 : 0.1 atomic weight ratios.

Samples with mixture of different phases (like 0.7 : 0.3 to 0.4 : 0.6 samples) showed combinations of dissociation peaks based on the amount of alane or alanate phase. As ~130 °C exothermic peak of calcium alanate and ~140 °C endothermic peak of alane, can affect the peak width in samples, DSC profiles gradually changed from two peak profile of alane to three peak profile of alanate.

The amount of hydrogen release in each dissociation steps can be calculated by TGA profiles shown in Fig. 7. Alane based samples (0.9 : 0.1 and 0.8 : 0.2) showed hydrogen contents about 8 wt% which is slightly smaller than alane phase in Al : Mg samples (~0.23wt% less). Formation of

Table 7: Dissociation activation energy for washed samples with 0.1 to 0.9 molar ratio of Ca.

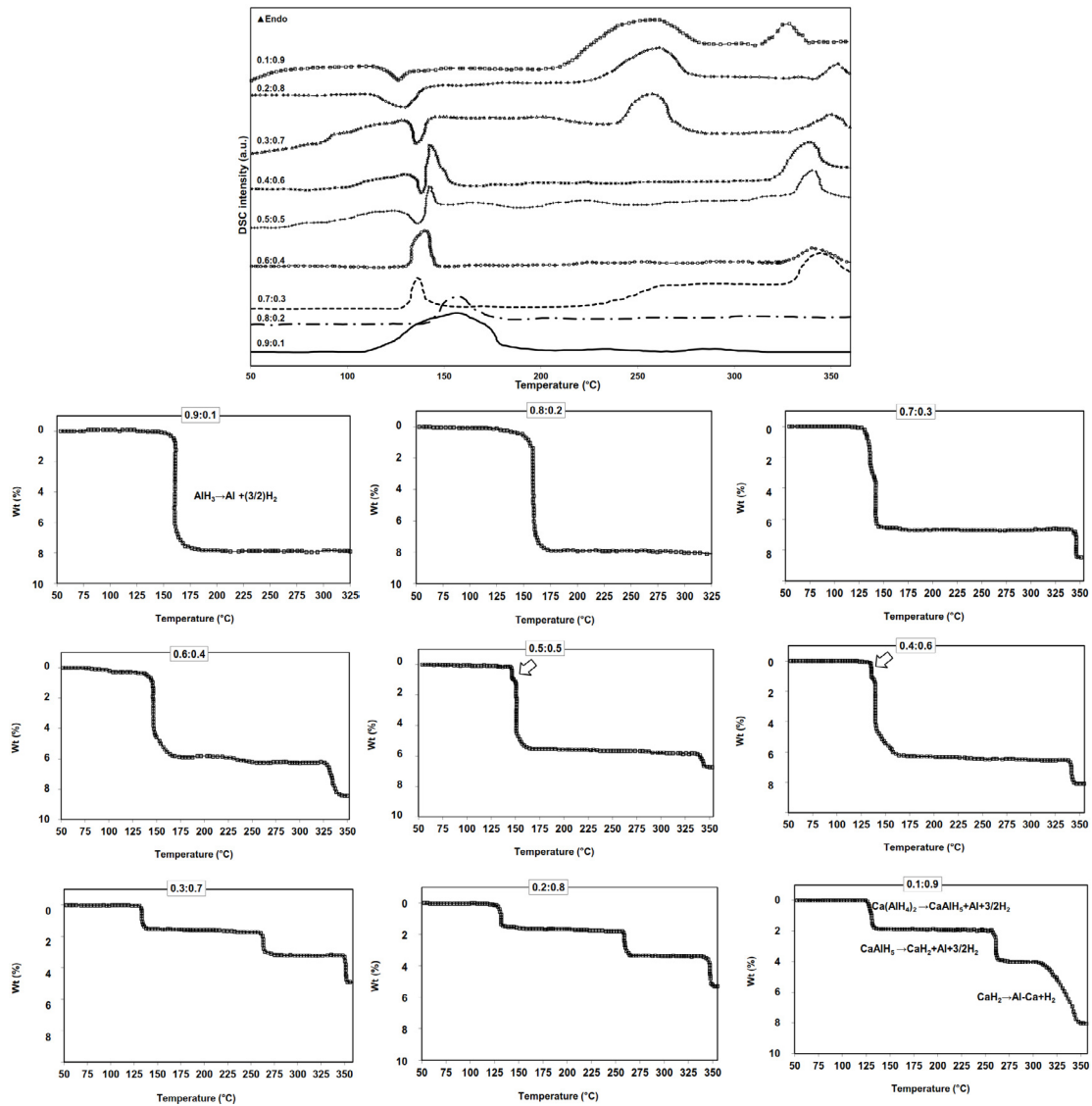| Sample (Al:Ca) | Activation energies (Ea) |
|---|---|
| 0.9:0.1 | 76 KJ/mol |
| 0.8:0.2 | 75 KJ/mol |
| 0.7:0.3 | 118 KJ/mol |
| 0.6:0.4 | 141 KJ/mol |
| 0.5:0.5 | 166 KJ/mol |
| 0.4:0.6 | 169 KJ/mol |
| 0.3:0.7 | ~90 KJ/mol |
| 0.2:0.8 | 90 KJ/mol |
| 0.1:0.9 | 92 KJ/mol |



Fig. 7: DSC and TGA patterns of Al : Ca samples from 0.9 : 0.1 to 0.1 : 0.9 atomic weight ratios.
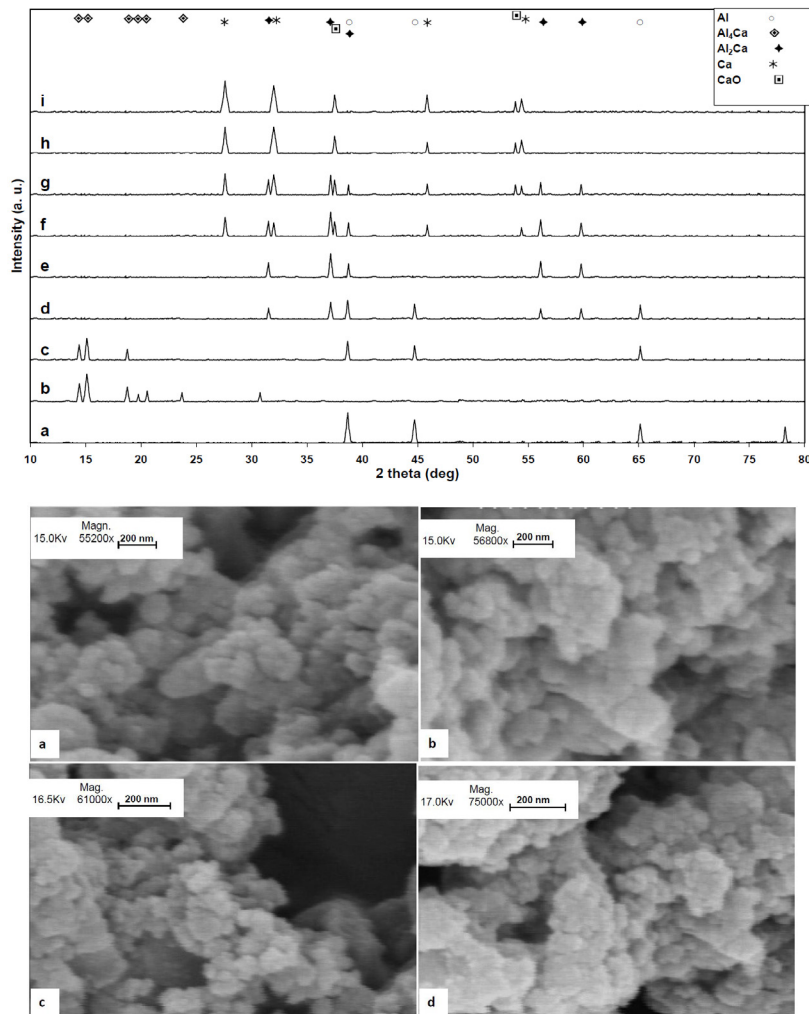
Fig. 8: XRD patterns of heated 0.1 to 0.9 calcium atomic weight ratio (a to i) samples and FE-SEM micrographs of Al:Ca=0.9:0.1 and 0.1 : 0.9 samples after washing process (a, b) and after heating process (c, d).

both alane and alanate phases in the samples (0.7 : 0.3 to 0.6 : 0.4) enhanced hydrogen content of the samples up to 8.7wt%. Calcium alanate phase (0.1 : 0.9) had hydrogen contents near 7.8wt%. Smallest amount of weight percent loss was detected in 0.3 : 0.7 sample. Small exothermic dissociation step of alanate in 0.5 : 0.5 and 0.4 : 0.6 is marked in plots, which was interrupted by endothermic dissociation of alane phase. Leading dissociation reactions for each step are shown in the inlets.

Same calculations for indicating dissociation activation energies using three heating rates and kissinger plots were carried out on these samples. Results are reported in Table 7. As mentioned, values are the combination of exothermic and endothermic dissociation steps for each sample.

Energies necessary for dissociation of alane phase was slightly lower than Al : Mg samples and about 75 kj/mol, while calcium alanate had larger activation energy near 92 kj/mol. As expected, samples with both alane and alanate phases showed higher activation energies up to 169 kj/molin 0.4 : 0.6 sample. The crystal structures of the products of the heating process were also analyzed using XRD shortly after dissociation. XRD profiles are shown in Fig. 8 for all samples. As seen, samples with lower contents of calcium were crystallized as aluminum based metals. Increasing calcium contents led to formation of aluminum – calcium intermetallics like $Al_4Ca$ and $Al_2Ca$ in 0.8 : 0.2 and 0.5 : 0.5 samples, respectively. Other samples were mostly combinations of Al, $Al_4Ca$ and $Al_2Ca$ phases. Formation of calcium free samples

Table 8: Crystal Structure, lattice parameters, lattice volume, lattice volume change percent, and calculated crystallite size of heated and samples with 0.1 to 0.9 molar ratio of Ca.

| Sample (Al:Ca) | Phase | Crystal Structure | Lattice parameters(Å) ±0.001 | $\Delta a/a_0$ (%) * | Lattice Volume(Å$^3$) ±0.0001 | $\Delta v/v_0$ (%)* | Crystallite size (nm) |
|---|---|---|---|---|---|---|---|
| 0.9:0.1 | Al | FCC | a= 4.040 | -0.22 | 65.94 | - 0.006 | 11 |
| 0.8:0.2 | Al$_4$Ca | FCC | a= 8.018 | - 0.02 | 515.8496 | ~ - 0.001 | 21 |
| 0.7:0.3 | Al | FCC | a= 4.038 | - 0.27 | 65.84 | - 0.008 | 12 |
|  | Al$_4$Ca | FCC | a= 8.019 | - 0.01 | 515.8496 | ~ -0.001 | 25 |
| 0.6:0.4 | Al | FCC | a= 4.045 | -0.10 | 66.18 | - 0.003 | 10 |
|  | Al$_2$Ca | FCC | a= 28.24 | 0.04 | 22521 | 0.001 | 18 |
| 0.5:0.5 | Al$_2$Ca | FCC | a= 8.021 | 0.01 | 516.0426 | ~ 0.00 | 18 |
| 0.4:0.6 | Ca | FCC | a= 5.589 | 0.02 | 174.5831 | ~ 0.00 | 13 |
|  | Al$_2$Ca | FCC | a= 8.021 | 0.02 | 516.0426 | ~ 0.00 | 19 |
| 0.3:0.7 | Ca | FCC | a= 5.590 | 0.04 | 174.6169 | 0.001 | 11 |
|  | Al$_2$Ca | FCC | a= 8.022 | 0.02 | 516.2356 | ~ 0.001 | 20 |
| 0.2:0.8 | Ca | FCC | a= 5.590 | 0.04 | 174.6169 | 0.001 | 12 |
| 0.1:0.9 | Ca | FCC | a= 5.591 | 0.05 | 174.7706 | ~ 0.001 | 14 |

\* regarding to standard pattern lattice parameters

started at 0.5 : 0.5 sample with Al$_2$Ca intermetallic phase accompanied by signs of calcium oxide (CaO). Formation of calcium oxide continued up to 0.1 : 0.9 sample as a byproduct due to high affinity of oxidation of calcium. More information on crystal structure is reported in Table 8. All phases (Al, Al$_4$Ca, Al$_2$Ca and Ca) had FCC crystal structure. As seen, most phases showed very small deviation from standard patterns, (lattice parameter and unit cell volume change) less than 0.05%, which indicates small amount of interstitial solid solutions or doping. These samples also showed small crystallite sizes about 10 – 25 nm. Intermetallic phases like Al$_4$Ca and Al$_2$Ca had slightly bigger crystallite sizes than metallic phases like Al or Ca.

FE-SEM studies of hydride and alanate samples showed formation of complex agglomerates of nano sized particles with irregular shapes. Micrographs of Al : Ca=0.9 : 0.1 and 0.1 : 0.9 are shown in Fig. 8(a,b) is an example of typical morphology of synthesized hydride and alanates and their shape after heating Fig 8(c,d). As seen, even at high resolutions, particle borders are hard to indicate. It seems that particle sizes were near 40-80 nm in hydride and alanate and slightly increased to 50-70 nm for alloyed samples.

## CONCLUSIONS

The effect of alkaline earth metals (magnesium and calcium) on formation of hydride /alanates and characteristics of synthesized nanopowders were studied using 0.1 atomic weight ratio step of aluminum: alkaline earth metal, with LiAlH$_4$ and aluminum/alkaline earth chlorides as precursors via mechano-chemical activation in

high energy ball mill. Constant increase in Mg and Ca contents from 0.1 to 0.9 atomic weight ratios slowly transformed the phases from modified alane to alanates with trigonal and monoclinic crystal structures. FTIR studies also confirmed different bonds formation in hydride and alanates due to formation of Al-H or alkaline earth metal-[AlH$_4$] bonds. The results of DSC/TGA analyses showed that thermal behavior was changed from the one step dissociation at ~150 °C with ~8.1 wt% hydrogen release in alane to the two steps hydrogen release in magnesium alanate at 130 and 285 °C with 7 and 2.1 wt% changes, and to the three steps hydrogen releases in calcium alanate at 127, 260, and 328 °C with 1.7, 2.1 and 4 wt% weight loss. Formation of controlled composition alloyed metals in Al-Mg, Mg-Al and intermetallics like Mg$_2$Al$_3$ and Mg$_{17}$Al$_{12}$ with no sign of oxides was detected in decomposed hydrides and alanates of Al: Mg system. Residual metals were pure aluminum, Al$_4$Ca, Al$_2$Ca intermetallic phases and Ca in aluminum: calcium system. Crystallite size of the samples was between 6 to 22 nm without any apparent trends and particle sizes near 60 nm.

## CONFLICT OF INTEREST

The authors declare that there is no conflict of interests regarding the publication of this manuscript.

## REFERENCES

[1] Bououdina M., Grant D., Walker G., (2006), Review on hydrogen absorbing materials-structure, microstructure, and thermodynamic properties. *Int. J. Hydr. Energy.* 31: 177-182.

[2] Sakintuna B., Lamari-Darkrim F., Hirscher M, (2007), Metal hydride materials for solid hydrogen storage: A review. *Int. J. Hyd. Energy.* 32: 1121-1140.

[3] George L., Saxena K., (2010), Structural stability of metal hydrides, alanates and borohydrides of alkali and alkali-earth elements: A review. *Int. J. Hydr. Energy.* 35: 5454-5470.

[4] Jain I. P., Jain P., Jain A., (2010), Novel hydrogen storage materials: A review of lightweight complex hydrides. *J. Alloys Compd.* 503: 303-339.

[5] Mamatha M., Bogdanovi B., Felderhoff M., Pommerin A., Schmidt W., Sch¨uth F., Weidenthaler C., (2006), Mechanochemical preparation and investigation of properties of magnesium, calcium and lithium–magnesium alanates. *J. Alloys Compd.* 407: 78-86.

[6] Sartori S., Istad-Lem A., Hendrik W., (2009), Mechano-chemical synthesis of alane. *Int. J. Hydr. Energy.* 34: 6350-6356.

[7] Fossdal A., Brinks H. W., Fichtner M. Hauback B. C., (2005), Determination of the crystal structure of Mg(AlH$_4$)$_2$ by combined X-ray and neutron diffraction. *J. Alloys Compd.* 387: 47-51.

[8] Paskevicius M., Sheppard D. A., Buckley C. E., (2009), Characterization of mechanochemically synthesized alane nanoparticles. *J. Alloys Compd.* 487: 370-376.

[9] Kumar S., Kain V., Kojima Y., (2017), Remarkably improved dehydrogenation of ZrCl$_4$ doped NaAlH$_4$ for hydrogen storage application. *Int. J. Hydr. Energy.* 42: 15299-15307.

[10] Pommerin A., Weidenthaler C., Schuth F., (2010), Direct synthesis of pure complex aluminium hydrides by cryomilling. *Scripta Materialia.* 62: 576–588.

[11] Yang C., Chen T., Tatsai W., (2012), Synergistic hydrogen desorption behavior of magnesium aluminum hydride synthesized by mechano-chemical activation method. *J. Alloys Compd.* 525: 126-132.

[12] Hosseinabadi N., Sarraf-mamoory S., Kaleji B. K., (2010), Synthesis, phase study and magnetic characterization of Co$_{50}$Fe$_{40}$Cu$_{10}$ ternary alloy nanopowders prepared by mechanochemical alloying process. *Powder Metall.* 53: 260-264.

[13] Pommerin A., Weidenthaler C., Schuth F., (2010), Influence of the ball milling conditions on the preparation of rare earth aluminum hydrides. *Scripta Materialia.* 63: 1128-1131.

[14] Fossdal A., Brinks H. W., Fichtner M., Hauback B. C., (2005), Thermal decomposition of Mg(AlH$_4$)$_2$ studied by in-situ synchrotron X-ray diffraction. *J. Alloys Compd.* 404–406: 752-756.

[15] Iosub V., Matsunaga T., Tange K., Ishikiriyama M., Miwa K., (2009), Synthesis of the hydride mixtures (1–x)AlH$_3$/xMgH$_2$ (0≤x≤0.3) by ball milling and their hydrogen storage properties. *J. Alloys Compd.* 484: 426-430.

[16] Iosub V., Matsunaga T., Tange K., Ishikiriyama M., (2009), Direct synthesis of Mg(AlH$_4$)$_2$ and CaAlH$_5$ crystalline compounds by ball milling and their potential as hydrogen storage materials. *Int. J. Hydr. Energy.* 34: 906-912.

[17] Liang F., Lin J., Wu Y. M., Wang L. M., (2017), Enhanced electrochemical hydrogen storage performance of TieVeNi composite employing NaAlH$_4$. *Int. J. Hydr. Energy.* 42: 14633-14640.

[18] Sato T., (Timmy) Ramirez-Cuesta A. J., Ikeda K., Orimo Sh., Yamada K., (2011), Vibrational properties of CaAlH$_5$ and r-AlH$_3$ with different AlH$_6$ networks studied by inelastic neutron scattering. *Inorg. Chem.* 50: 8007-8011.

[19] Kumar S. Jain A., Miyaoka H., Ichikawa T., Kojima Y., (2017), Catalytic effect of bis (cyclopentadienyl) nickel II on the improvement of the hydrogenation dehydrogenation of Mg-MgH$_2$ system. *Int. J. Hydr. Energy*. 42: 17178-17183.

[20] Cheetham A. K., (1995), The rietveld method, edited by R.A. Young, oxford: oxford unvpress.